Green Chemistry

Cutting-edge research for a greener sustainable future

rsc.li/greenchem

Waste PET plastic

Carbonization

Activation

CO₂-free gas

CO₂-rich gas

Porous carbon

PSA

ROYAL SOCIETY
OF CHEMISTRY

PAPER
Shauhrat S. Chopra, Hankwon Lim, Yong Sik Ok *et al.*
Sustainability-inspired upcycling of waste polyethylene
terephthalate plastic into porous carbon for CO₂ capture

PAPER

Check for updates

Sustainability-inspired upcycling of waste polyethylene terephthalate plastic into porous carbon for CO_2 capture†

Xiangzhou Yuan, ‡[a,b] Nallapaneni Manoj Kumar, ‡[c] Boris Brigljević, ‡[d,h] Shuangjun Li,[e] Shuai Deng,[e] Manhee Byun,[d] Boreum Lee,[d] Carol Sze Ki Lin,[c] Daniel C. W. Tsang,[f] Ki Bong Lee,[g] Shauhrat S. Chopra, *[c] Hankwon Lim *[d] and Yong Sik Ok *[a]

In addition to climate change, plastic pollution is widely recognized as one of the most severe environmental concerns. Waste plastic-derived advanced materials for carbon capture provide promising solutions to these environmental issues. However, the environmental sustainability and economic feasibility of such a novel approach are still unclear for it to be implemented on an industrial scale globally. As synthesis routes differ in terms of their environmental impact and economic feasibility, we synthesized three waste polyethylene terephthalate (PET) plastic-derived porous carbons (PET6-CO2-9, PET6-K7, and PET6-KU7) using physical and chemical activation routes. The resulting porous carbons exhibited high CO_2-capture capacities. Based on techno-economic and life-cycle assessments of the scaled-up industrial processes, we showed that the physical CO_2 activation approach performs the best in the reduction of carbon emissions, providing the possibility for carbon neutrality while exhibiting financial viability (net present value of at least €19.22 million over the operating life of the project). Owing to the environmental benefits and economic feasibility of this approach, we highlighted its potential as a multifunctional alternative to conventional CO_2 absorption and plastic waste management technologies.

Introduction

The valorization of solid plastic waste into advanced materials for carbon capture provides the benefit of mitigating both plastic pollution and climate change issues.[1,2] Currently,

[a]*Korea Biochar Research Center, APRU Sustainable Waste Management Program & Division of Environmental Science and Ecological Engineering, Korea University, Seoul 02841, Republic of Korea. E-mail: yongsikok@korea.ac.kr*
[b]*R&D Centre, Sun Brand Industrial Inc., Jeollanam-do 57248, Republic of Korea*
[c]*School of Energy and Environment, City University of Hong Kong, Tat Chee Avenue, Kowloon, Hong Kong, China. E-mail: sschopra@cityu.edu.hk*
[d]*School of Energy and Chemical Engineering, Ulsan National Institute of Science and Technology, 50 UNIST-gil, Eonyang-eup, Ulju-gun, Ulsan 44919, Republic of Korea. E-mail: hklim@unist.ac.kr*
[e]*Key Laboratory of Efficient Utilization of Low and Medium Grade Energy (Tianjin University), Ministry of Education of China, Tianjin, China*
[f]*Department of Civil and Environmental Engineering, The Hong Kong Polytechnic University, Hung Hom, Kowloon, Hong Kong, China*
[g]*Department of Chemical and Biological Engineering, Korea University, Seoul 02841, Republic of Korea*
[h]*Carbon Value Co., Ltd., 2801 A–dong, 97, Centum Jungang–ro, Haeundae–gu, 48058 Busan, Republic of Korea*
†Electronic supplementary information (ESI) available. See DOI: 10.1039/d1gc03600a
‡These authors contributed equally as first authors.

plastic pollution is a critical cause of global environmental changes,[3–5] owing to the irreparable and ubiquitous widespread damage to ecosystems,[6] including adverse effects on crop productivity[7] and clean water sources.[8] Climate change has received global attention owing to the ever-increasing concentrations of atmospheric carbon dioxide (CO_2).[9,10] Carbon capture and storage (CCS) has been highlighted as a promising solution to achieve efficient decarbonization to mitigate climate change.[11,12] Greenhouse gas removal (GGR) has also been considered for climate change mitigation.[13] This suggests that deploying CCS and GGR technologies is integral to meeting climate change and sustainable development goals (SDGs). However, the CO_2 capture process is still considerably expensive (accounting for up to 50%–80% of total CCS costs[1]) and, thus, cannot be commercially deployed on a large scale. Among the existing CO_2 capture technologies, porous-carbon-based adsorption has been prioritized for carbon capture deployment,[1,2] owing to its cost-effectiveness, mild operating conditions, high deployment feasibility, and low energy consumption. The lab-scale syntheses of low-cost porous carbons exhibiting high CO_2 adsorption performance by using waste polyethylene terephthalate (PET) plastic bottles, an abundant and carbon-rich source with low global recycling rates (~10% [14]), have been started in 2019.[1,2,15–18]

Various synthesis routes for preparing porous carbons (such as biomass-derived) for CO_2 capture have been extensively studied,[1,15,19–24] substantiating that porous carbons are usually synthesized by carbonization followed by physical or chemical activation. Physical activation is an environmentally friendly method of producing porous carbons, using steam or CO_2 as an activating agent; however, such porous carbons have poor textural properties.[19–21] In contrast, chemical activation usually produces porous carbons with high porosity and a well-developed pore structure, which are desirable qualities for CO_2 capture; however, the process involves the use of hazardous chemical agents (such as potassium hydroxide and zinc chloride).[22–24] In addition, doping with nitrogen (N)-based agents (such as urea, melamine, and sodium amide) is generally performed to enhance CO_2 uptake and selectivity.[18,25] To address the limitations of existing techniques, the trade-offs between different synthesis routes and their corresponding environmental costs should be comprehensively evaluated to develop more sustainable and feasible waste PET plastic-based CO_2 capture processes. Therefore, we synthesized three waste PET plastic-derived porous carbons (WPDPCs) using CO_2 physical, KOH chemical, and KOH/urea chemical activation processes.

The primary steps in establishing an emerging technology are the synthesis and simulation of a process outside the laboratory, to justify its improved sustainability and cost-effectiveness. Combined with experimental data, preliminary process designs could be further upscaled and optimized, thereby providing vital information (including energy and mass balance, thermodynamic efficiency, and carbon emissions) that can serve as a realistic basis for the analysis of the economic and environmental aspects. Process simulation has been used in various research areas such as oil and gas,[26] chemical synthesis,[27,28] biomass utilization,[29,30] and renewable energy.[31–33] This approach was best exemplified in a feasibility study on solar steam methane reforming techniques,[31] in which emerging and established technologies were combined. The technical, economic, and environmental factors were evaluated for different combinations of volumetric receiver reactors, molten salts, solar thermal power generation, and water electrolysis capabilities. Multiple liquid organic hydrogen storage systems, an emerging concept in hydrogen storage, were recently assessed to determine market uncertainty at the industrial-scale,[34] where underlying process simulation models were the key tools that allowed for reasonable quantitative comparisons. To analyze the energy and environmental efficiency of this process strictly in the context of systems having a similar size and function, the results from our study can be compared, for instance, with those of a previous study[35] in which an energy analysis was conducted to evaluate the feasibility of using CCS technology in fossil-fuel-based power plants.

The overall goal of this study was to compare the usefulness of alternative pathways with significant potential to sequester carbon for the sustainable and economically viable production of carbon capture materials derived from waste PET plastic.

The three objectives to ensure the selection of the appropriate technology were to (1) evaluate and verify the steady-state CO_2 capture performance of porous carbon from the feeding gas (20 vol% CO_2 balanced with N_2) using a 5-step temperature vacuum swing adsorption (TVSA) process, (2) determine the economic sustainability of the scaled-up industrial process using techno-economic assessment (TEA), and (3) quantify the production pathways and global warming potentials (GWPs) of alternative porous carbon production pathways using gate-to-gate life-cycle assessment (LCA). Sensitivity analysis methods that incorporate the WPDPC prices and the conversion ratios of heat-to-power were also used to determine the revenue generated by the scaled-up industrial processes while highlighting the factors that are expected to significantly influence key economic parameters. A simplified Ashby plot was created based on the integrated TEA and LCA results to facilitate the selection of appropriate WPDPC production technologies. The findings of this study are expected to guide decision-making for the early adopters of alternative production pathways in terms of capital intensity and performance optimization and the policymakers concerned with the environmental impacts of plastic waste. Most importantly, to meet the SDGs established by the United Nations,[36] the upcycling of WPDPCs for CO_2 capture might be verified as a promising and sustainable route (Fig. 1a), because this technique is beneficial to not only simultaneously mitigate climate change (SDG 13: climate action) and plastic pollution (SDG 14: life below water and SDG 15: life on land), but also facilitate the sustainable recycling of discarded PET plastic bottles in urban areas (SDG 11: sustainable cities and communities and SDG 12: responsible consumption and production).

Methods

Lab-scale sample preparation

PET plastic bottles were collected from our daily surroundings (such as garbage cans and streets) as the source material for synthesizing porous carbons. Before carbonization and activation/modification were performed, the bottles were pretreated by removing the bottle caps and labels, washing, drying, and cutting into small pieces (approximately 5 mm × 5 mm). The PET sample was carbonized at 600 °C for 1 h in a N_2 atmosphere using a horizontal cylindrical furnace. The carbonized sample (PET6) was then used to synthesize three porous carbons (the WPDPCs) by employing different activation methods (Fig. 1b). The first porous carbon, PET6-CO_2-9, was synthesized by CO_2 activation at 900 °C for 2 h under a CO_2 flow rate of 200 mL min^{-1}. The second porous carbon, PET6-K7,[18] was prepared by KOH activation at 700 °C for 1 h under a N_2 flow rate of 200 mL min^{-1}, and the mass ratio of KOH : PET6 was 2 : 1. The third porous carbon, PET6-KU7,[18] was developed using a one-pot synthesis method at 700 °C for 1 h under a N_2 flow rate of 200 mL min^{-1}, with the mass ratio of KOH : urea : PET6 set at 2 : 1 : 1. The details of the synthesis of porous carbons from PET plastic are provided in the ESI.†
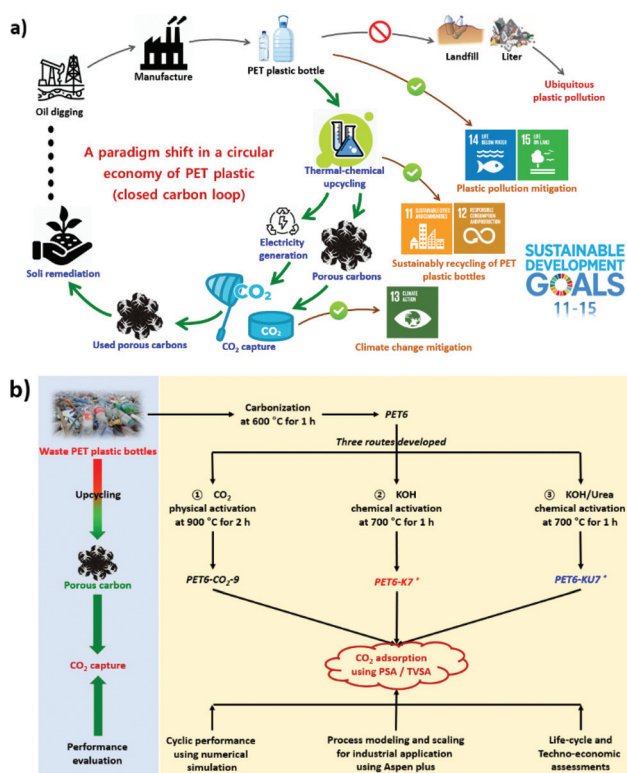
Fig. 1 (a) Upcycling waste polyethylene terephthalate (PET) plastic bottles into porous carbons for CO_2 capture as proposed in a large-scale study, and this can aid in achieving the United Nations Sustainable Development Goals (SDGs)[36] and (b) schematic diagram of the production of waste PET plastic-derived porous carbons (WPDPCs) using three different activation routes. * The synthesis methods of both PET6-K7 and PET6-KU7 were derived from previous publications.[18] PSA: pressure swing adsorption; TVSA: temperature vacuum swing adsorption.

Steady-state modeling

To effectively screen porous carbons prepared for practical CO_2 capture, a cyclic performance evaluation using the TVSA process was conducted.[37] A 5-step (pressurization, adsorption, heating, vacuuming, and cooling) TVSA system (Fig. S1†) was designed using the three WPDPCs. All the parameters and recorded physical phenomena are listed in Tables S1 and S2,† respectively. The CO_2 gas was captured and separated from the mixed gases using temperature- and pressure-driven adsorption and desorption processes. The adsorption chamber with the CO_2 adsorbents and gases were considered as a single system to simplify the process to steady-state approximations; the numerical simulation was run on MATLAB (MathWorks, USA). The assumptions employed are as follows: (1) the gas inside the adsorption chamber is an ideal gas, (2) the pressure drop across the adsorption chamber can be ignored, (3) the mass transfer resistance between the solid and gas phases can be ignored, (4) the temperature of the adsorption chamber is homogeneous, and (5) the physical properties of the system under consideration (specific heat capacity, density, and void fraction) remain constant. More details of the assumptions

used to simplify the system in the steady-state simulation can be found in previously published studies.[38,39] Based on the aforementioned assumptions, the mass and energy balance equations of the system were formulated, and the governing equations are listed in Table S3.† Specific unknowns (such as temperature or pressure variation with time throughout the process) were calculated for further analysis (Fig. S2†).

Process modeling and methodology

The steady-state synthesis process models for all three WPDPCs (PET6-CO_2-9, PET6-K7, and PET6-KU7) were simulated using Aspen Plus (v11) flowsheet simulation software. Waste PET plastic, PET6, PET6-CO_2-9, PET6-K7, and PET6-KU7 were modeled as non-conventional solids, with their proximate and ultimate analyses as the primary inputs, using a specialized property method named SOLIDS,[40] which is well-suited to modeling coal-based and pyrometallurgical processes. Owing to the presence of organic acids, process sections that utilized vaporized pyrolysis liquids and waxes and non-condensable gases were modeled using a non-random two-liquid (NRTL) activity coefficient model for the liquid phase and the Hyden O'Connell[41] equation-of-state for the vapor phase. The Rankine steam cycle was modeled using the STEAM-TA property method, which utilizes the 1967 American Society of Mechanical Engineers steam table correlations.[42] As the working fluid in the organic Rankine cycle (ORC) was iso-butane,[43] the Soave–Redlich–Kwong[44,45] equation-of-state property method was used, as it is applicable to modeling pure hydrocarbon systems. All other process sections were modeled using the NRTL-Redlich–Kwong equation-of-state.

The ultimate analysis of the PET feedstock was calculated as an average normalized value based on previously published studies on pure PET samples[46–54] (Table S4†). The compositions of the liquid and waxy products from the slow pyrolysis of waste PET plastic at 600 °C were confirmed based on the literature[55–57] and tuned to the correct atomic balance of this process (Table S5†). The thermal energy required for the slow pyrolysis of waste PET plastic was estimated by integrating a differential scanning calorimetry trace of pure PET plastic (Fig. S3†) that was obtained from the NETZSCH-Gerätebau GmbH company instrument application sheet.[58] The total thermal energy estimated for waste PET plastic thermal decomposition (5 °C min⁻¹ to 600 °C + 1 h at 600 °C) was 2.57 MJ kg⁻¹. A parametric sensitivity analysis with varying air-to-fuel (ATF) ratios was performed to ensure complete combustion of the PET liquid and vapor products (Fig. S4†). The lower heating value of the pyrolysis vapor products mixture was determined to be 19.22 MJ kg⁻¹, with complete combustion achieved at an ATF ratio of approximately 9.2 (wt/wt), which was observed when the CO level reached zero. Nevertheless, an ATF ratio of 14 was set as the operating value to reduce the possibility of volatile organic carbon emissions.

LCA methodology

A gate-to-gate LCA of the three activation methods used to produce porous carbon materials was modeled to compute the

environmental impact categories for the amounts of the different materials (CO_2, KOH, urea, and HCl) used in each activation process (Table S6†). The life-cycle GWP, fine particulate matter formation, and other impact categories (Table S7†) of the carbon activation processes were calculated using the ReCiPe (H) Midpoint method in SimaPro (v8.5.2) software. The functional unit (FU) is a fundamental aspect of LCA studies, and a straightforward unit, such as "kg-kilogram" and "g-gram", is typically selected in most studies. In this study, the FU was chosen based on the function or service of the adsorbent material. Therefore, the FU was "kg of CO_2 captured by waste PET-derived porous carbon". The life-cycle inventories (LCI) of the carbon activation processes and other material inputs were obtained from the LCI databases such as Ecoinvent 3,[59] Agri-footprint,[60] and Industry data 2.0.

TEA methodology

The TEA model was developed by considering the capital investment, operational expenses, and revenues generated for the scaled-up process modeling of the three adsorption materials. The porous carbon production plant was expected to operate for 15 years (n) with an annual running time (t) of approximately 8000 h. The capital investments and operational expenses for 1 t h^{-1} of WPDPC production are presented in Tables S8 and S9.† These costs were categorized as a total capital investment (TCI), yearly operational cost (YOC), and total plant cost (TPC). The revenue was generated from a scaled-up production unit. To generate revenue, the porous carbon could be sold at market prices depending on the region and/or the electricity produced by the combined heat and power (CHP) plant. The optimized process design estimated a net power between 710.51 kW h and 733.24 kW h, depending upon the activation process used. Therefore, the total revenue (TR) earned by selling the produced activated biochar and the CHP plant's excess electricity was accounted for in the TEA model at Chinese market-driven prices (Table S10†) to obtain the net cash flow for the years of operation. When the revenues were estimated, the varying market prices and heat-to-power conversion losses were considered over the lifetime of the process. A total of 75 scenarios was derived by varying the porous carbon sales and heat energy available for power generation (Tables S11–S13†).

To evaluate the revenue, we used the two best possible avenues: (1) by selling the WPDPCs in the market,[61] as the market price can vary,[62] different scenarios of porous carbon sales were considered and modeled (eqn (1)) and (2) by selling electricity at the feed-in tariff rates (eqn (2)):[61,63]

$$R_{PC} = \sum_{t=1}^{n} Q_{PC} \times SP_{PC},$$

$$\begin{cases} SP_{PC} < \min MP_{PC} \\ SP_{PC} = \min MP_{PC} \\ SP_{PC} = \max MP_{PC} \\ SP_{PC} = \text{avg} \, MP_{PC} \\ \min MP_{PC} < SP_{PC} < \text{avg} \, MP_{PC} \end{cases} \quad (1)$$

where R_{PC} is the revenue obtained from porous carbon (PC), Q_{PC} is the quantity of PC produced in tons, and SP_{PC} is the selling price of the PC per ton in Euros (minimum, max, and average).

$$R_E = \sum_{t=1}^{n} U_E \times \text{FiT}_E, \quad (2)$$

where R_E is the revenue obtained from electricity (E), U_E is the units of electricity produced in kW h for different heat-to-power conversion ratios after considering heat losses (1%, 10%, 20%, 50%, and 75%). FiT_E is the feed-in tariff for a unit of electricity in Europe.

The TR generated is the sum of revenues earned by selling porous carbon and electricity, and it is calculated using eqn (3):[61]

$$\text{TR} = R_{PC} + R_E. \quad (3)$$

Numerous economic indicators (discounted payback period (DPBP) in years, net present value (NPV) in one million euros, internal rate of return (IRR) in percentage, and simple payback period (SPBP) in years) were estimated to understand the economic viability of the three-production process. A positive NPV, low DPBP and SPBP, and high/positive IRR were considered to be good indicators that favored investment in a given industrial project. These indicators also serve as readouts of the TEA model's desired outcome, which can be viewed as a useful indicator of the porous carbon production unit's profitability assessment. The DPBP denotes the time needed to recover the initial investment for possible discount rates (10%).

The mathematical expressions used to estimate the economic indicators, NPV, IRR, SPBP, and DPBP, are described in eqn (4)–(7),[62,63] respectively.

$$\text{NPV} = \sum_{t=1}^{n} \frac{\text{TR} - \text{YOC}}{(1 + \text{DR})^t} - \text{TCI}, \quad (4)$$

$$0 = \sum_{t=1}^{n} \frac{\text{TR} - \text{YOC}}{(1 + \text{IRR})^t} - \text{TCI}, \quad (5)$$

$$\text{SPBP} = \frac{\text{TCI}}{\text{net annual cash flows}}, \quad (6)$$

$$\text{DPBP} = \text{year before DPBP occurs}$$
$$+ \frac{\text{CCF in the year before recovery}}{\text{DCF in the year after recovery}}, \quad (7)$$

where CCF and DCF are the cumulative cash flow and discounted cash flow in millions of euros, respectively.

Results

CO_2 uptake of PET plastic-derived porous carbons

We synthesized three types of WPDPCs (PET6-CO_2-9, PET6-K7, and PET6-KU7) using three different optimized activation routes (Fig. 1b); scanning electron microscopy (SEM) images (Fig. S5a†) revealed no distinct morphological differences

between the WPDPCs. Among all the samples prepared (Fig. S5b and Table S14†), only PET6-KU7 displayed N content of 3.23 wt%,[18] verifying that the N-doping treatment was effective. The D peak at 1350 cm^{-1} and G-peak at 1589 cm^{-1} were observed in the Raman spectra (Fig. S5c†).[18,64] Similar intensity ratios of the D and G bands (I_D/I_G = ~1.0) were obtained for all three samples, indicating that the degree of graphitization of the WPDPCs did not differ significantly across the different activation routes. As per the International Union of Pure and Applied Chemistry classification system, the N$_2$ adsorption–desorption isotherms (Fig. S5d†) were categorized as type I, suggesting that the prepared samples are typical microporous carbon materials. As shown in Fig. S5e,† different peaks were detected for each sample, and the micropores were well developed in all WPDPCs. The dominant pore size was <1.5 nm, which is suitable for CO$_2$ capture.[65] As shown in Fig. 2a–c, we evaluated the CO$_2$ adsorption performance of the three porous carbons under 1 bar at 0, 25, and 50 °C, as summarized in Table S14.† The isosteric heat of adsorption (Q_{st}) (Fig. 2d) was calculated using the Clausius–Clapeyron equation (eqn (S1)†). For each sample, we plotted ln (P) versus $1/T$ for the CO$_2$ adsorption isotherms obtained at 0, 25, and 50 °C. Dynamic CO$_2$ adsorption within 2 h was also assessed using thermogravimetric analysis (TGA) at 30 °C and 1 bar (Fig. 2e); over 95% of the total CO$_2$ uptake by each sample was achieved within the first 5 min, indicating fast adsorption kinetics. Moreover, the cyclic stability of each prepared sample was evaluated using ten adsorption–desorption cycles at 30 °C and 1 bar (Fig. 2f). Identical cycle curves of the CO$_2$ adsorption and desorption processes were obtained for each type of porous carbon. We also observed stable working capacities of 2.68 mmol g^{-1} for PET6-CO$_2$-9, 3.03 mmol g^{-1} for PET6-K7,[18] and 3.28 mmol g^{-1} for PET6-KU7;[18] substantially higher than that of industrial-scale aqueous monoethanolamine absorption (1.5 mmol g^{-1}).[66] Desorption was easily achieved by switching the purging gas from the target gas to N$_2$.

Steady-state cyclic performance evaluation

A steady-state numerical simulation of the 5-step TVSA process (Fig. S1†) of the WPDPCs was conducted, and their cyclic performance was evaluated. From the industrial application and energy consumption perspective, five major indicators, including productivity, purity, recovery, specific consumption, and exergy efficiency, were considered when selecting porous carbons with optimal CO$_2$ capture performance.[67,68] Based on the detailed operating parameters (Table S15†), the steady-state cyclic performance of the WPDPCs was evaluated using numerical simulations. The major outcome (Table S15†) was that, compared with PET6-CO$_2$-9 and PET6-K7, PET6-KU7 appeared to be the most promising candidate for CO$_2$ capture from the perspective of industrial application and energy consumption.

Scale-up for industrial CO$_2$ capture

We scaled up our novel processes to industrial applications based on lab-scale experimental data. For all three processes
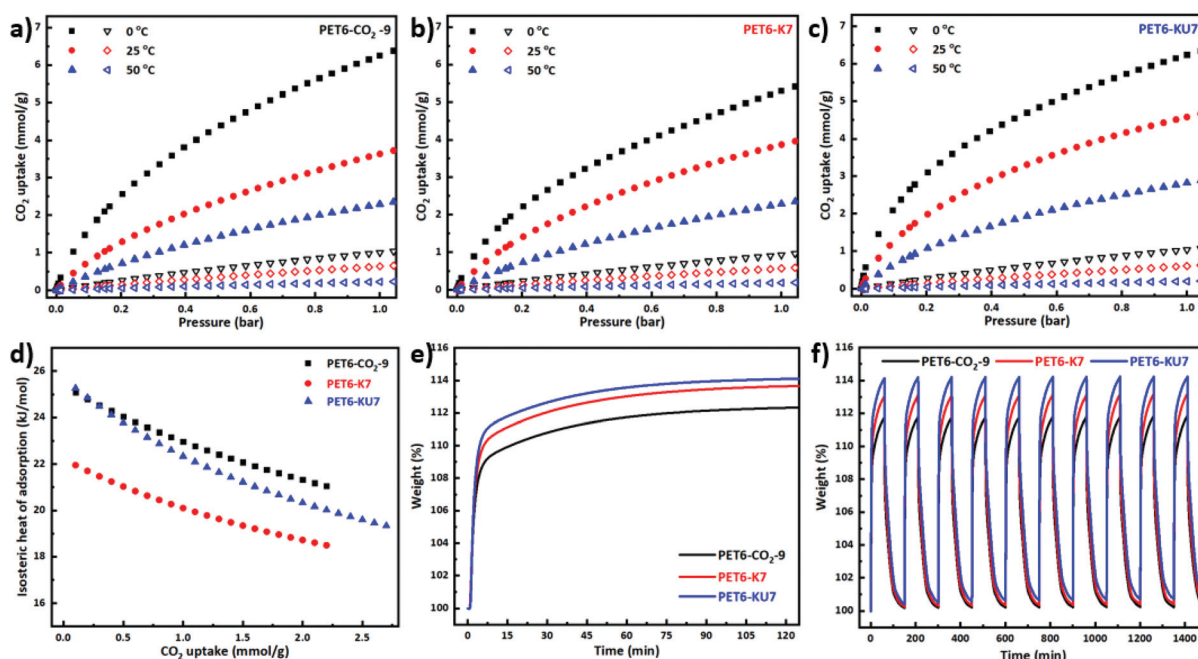

Fig. 2 Comparisons of CO$_2$ and N$_2$ adsorption isotherms of the three WPDPCs: (a) PET6-CO$_2$-9, (b) PET6-K7 and (c) PET6-KU7, at three different temperatures (solid and open symbols represent CO$_2$ and N$_2$ adsorption, respectively). (d) Isosteric heat of adsorption (Q_{st}) for waste PET plastic-derived samples estimated from the CO$_2$ adsorption isotherms at 0 °C, 25 °C, and 50 °C. (e) Dynamic CO$_2$ adsorption and (f) 10 cyclic CO$_2$ adsorption–desorption tests using thermogravimetric analysis (TGA) at 30 °C and 1 bar. Note that all data for PET6-K7 and PET6-KU7 were derived from a previous publication.[18]
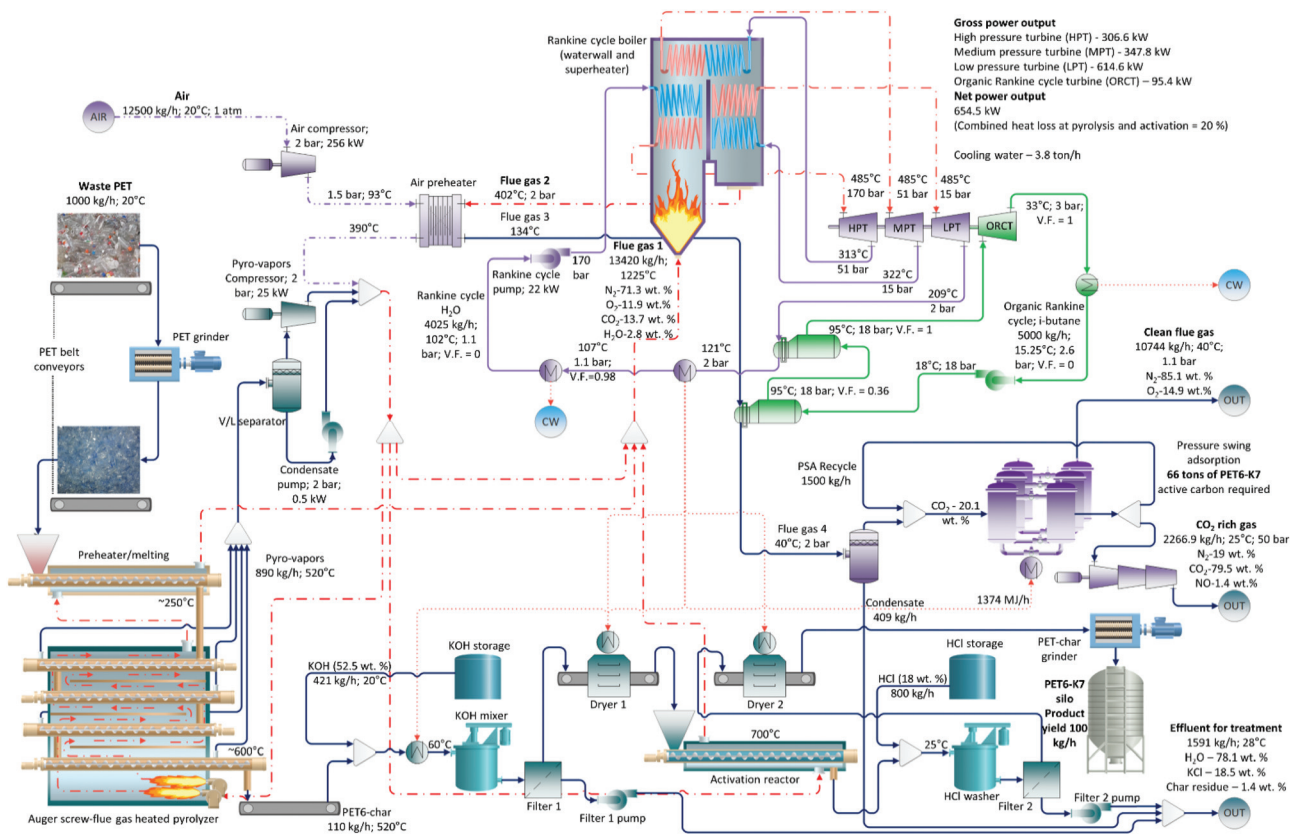
Fig. 3 Process flow diagram of the PET6-K7 porous carbon production process and flue gas CO_2 capture of a representative 1 t h^{-1} PET waste scale. Blue streamlines and unit operations indicate pyrolysis and activation processes. Purple streamlines and operations indicate the primary power (Rankine) cycle and CO_2 capture. Green streamlines indicate the secondary power (organic Rankine) cycle and a heat sink for the flue gas before the CO_2 capture process. Red streamlines indicate primary heat sources for the process (lines and dots) and major heat duties of the unit operations (dots only).

(PET6-CO$_2$-9 shown in Fig. S6,† PET6-K7 in Fig. 3, and PET6-KU7 in Fig. S7†), the first step was to grind the as-received waste PET plastic bottles as feedstock at a feeding rate of 1 ton per h for comprehensive comparisons. A belt conveyor fed the waste PET flakes into a preheating/melting extruder, where the PET melted at approximately 250 °C (as indicated in Fig. S3†). The melted PET was then fed into a cascading auger-screw pyrolyzer that gradually increased the temperature of the material as it traveled slowly downward. The thermal energy used in the pyrolyzer and preheating extruder was provided by a countercurrent flow of hot flue gas produced at the bottom of the pyrolyzer by a series of gas burners. All auger tubes of the pyrolyzer were under negative pressure, which caused volatiles and gases (890 kg h^{-1}) to be transported to a temporary storage drum (a vapor–liquid separator). The assumed heat losses lowered the temperature of the pyrolysis products from 600 °C to 520 °C during transportation. Approximately 12.5 t h^{-1} of air was compressed and heated to 390 °C in an air preheater. A combustion mixture of hot air and pyrolysis products was then utilized for three major sinks of high-temperature heat: the pyrolyzer, activation reactor, and Rankine cycle boiler. Eventually, all combustion products were utilized in the Rankine cycle as they vaporized and superheated the steam.

Approximately 4 t h^{-1} of water was utilized in the Rankine cycle for electricity generation. After the last turbine expansion, the hot water/steam mixture at 209 °C and 2 bar first transferred heat in the ORC boiler and then emitted heat to meet the unit operation requirements of preheating, drying, and desorption. The steam was completely reliquified in a cooling water condenser, after which it was compressed to a maximum pressure of 170 bar to restart the cycle. The flue gases exited the Rankine cycle boiler at 400 °C and were used to preheat the combustion air, which cooled the gases down to 135 °C. This temperature was too high for CO_2 capture using the pressure swing adsorption (PSA) system and would require a large amount of cooling water to reduce the temperature below 50 °C (owing to the sheer flow rate of the flue gas). Therefore, an ORC was introduced to utilize this large amount of waste heat. The ORC working fluid (5 t h^{-1} of isobutane) was compressed to 18 bar and entered the first reboiler at 18 °C, where it absorbed the flue gas heat and cooled the gas to 40 °C. As it exited the reboiler, the isobutane had a vapor fraction of only 36%; therefore, the heat needed to achieve total vapor was provided by the Rankine cycle hot water in the second reboiler. The ORC turbine expanded the isobutane to 3 bar and generated 95 kW of work, after which it was con-

densed to liquid at 15.2 °C and was recompressed. In all the cases, the total gross power generated from the combined power cycles was approximately 1.36 MW or 0.71–0.73 MW net when all unit operations were considered. The cooled flue gas was first separated from the condensed water in a flash drum, after which the CO_2 was separated using a series of PSA beds that utilized the three WPDPCs. The amount of PSA adsorbent bed material (calculated from the flue gas composition, flow rate, and experimental isotherms) necessary for complete CO_2 separation varied from 46 to 76 tons based on the activation route. The CO_2-rich gas was compressed to a pipeline pressure of 50 bar and was removed from the process either as a secondary product or for storage.

The CO_2-rich gas (74.2 wt%) was transported at a rate of 1416 kg h^{-1} into the activation reactor operating at 900 °C to synthesize the PET6-CO_2-9 sample (Fig. S6†). The gases from the reactor were sent to the combustion chamber of the Rankine cycle boiler, where the product (88 kg h^{-1}) was powdered and stored. The PSA system required 76 tons of adsorbent material; as a result, the process had to run for 36 days (= 76 000 kg (88 kg h^{-1} × 24 h day^{-1})$^{-1}$) to produce the required quantity. To prepare the PET6-K7 sample (Fig. 3), PET6 (110 kg h^{-1}) was transported into a mixing vessel and was mixed with a KOH solution (421 kg h^{-1}; 400 g L^{-1}) at 60 °C. The liquid was then separated using a filter, and PET6 was dried in a convective dryer before entering the activation reactor. Activation occurred at 700 °C, after which an HCl solution (800 kg h^{-1}, 5 M) was used to remove residual KOH from the porous carbon. Finally, the liquid was filtered, and the finished product (100 kg h^{-1}) was dried, ground into a powder, and stored. The processing time required to achieve the calculated PSA system requirement of ~66 tons was 28 days. The process required to develop PET6-KU7 (Fig. S7†) were the same as those used to develop PET6-K7, except that PET6 was mixed with KOH and urea (230 kg h^{-1}). The final product yield was 90 kg h^{-1}, and the PSA requirement was ~46 tons, which translated to 21 days of operation.

Environmental impact and economic benefit

We compared the environmental impacts of the three activation pathways used to produce WPDPCs. The LCA modeling results revealed that the KOH/urea chemical activation pathway had larger environmental impacts in almost all of the selected 18 impact categories, which was approximately 200% higher than the CO_2 physical activation pathway and −1.74% to 125% higher than those of the KOH chemical activation pathway (see Fig. S8a and S9† for details and mitigated environmental impacts are provided in Fig. S8b†). Among all the impact categories, GWP is arguably the most important. The CO_2 physical activation pathway had the lowest GWP, and the KOH/urea chemical activation pathway had the highest GWP (Fig. 4 and 5a). The TEA results revealed various viable scenarios for producing industrial-scale porous carbons. The NPV was calculated for the production of each of the WPDPCs in different scenarios by varying the heat-to-power conversion losses and selling prices of the porous carbons. Each scenario
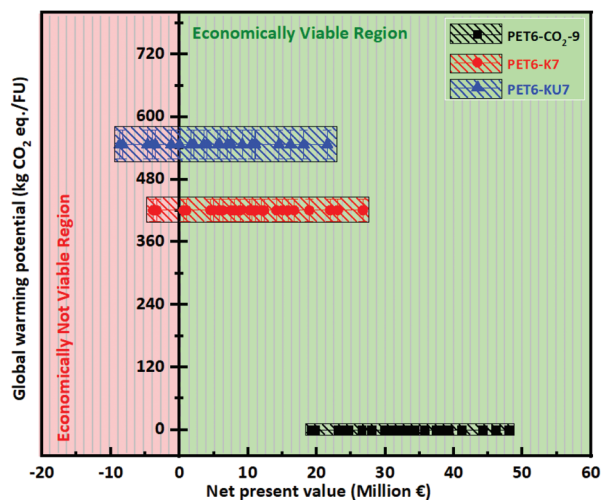

Fig. 4 Environmental impact and economic benefit of the three WPDPCs. The global warming potential (GWP) and the net present value (NPV) shown here have been quantified as part of this study. The boxed regions represent the possible range for the GWP and NPV of the three WPDPCs. For the porous carbons, the black box embedded with blue triangles represents PET6-KU7, which has higher environmental impacts; the black box embedded with red circles represents PET6-K7, which has lower environmental impacts than PET6-KU7; and the black box embedded with black squares represents PET6-CO_2-9, which has the lowest environmental impacts. The variation in the NPV depends on the selling price of porous carbon and the electricity sales associated with the industrial-scale waste PET plastic bottle treatment facility; using this, we identified the viable (positive NPV, represented by the green region of the plot) and non-viable (negative NPV, represented by the red region) options for producing porous carbons.

accounted for the capital investment in the plant, operational expenses for 15 years, and revenues earned from the sale of porous carbon and electricity produced from the processes. The results revealed PET6-CO_2-9 production to be the most feasible process, followed by PET6-K7 and PET6-KU7 production (Fig. 4). The TEA results suggested that all three pathways could produce porous carbons, even with 20% energy loss during the process and the sale of products at the lowest market price, that is, €200 per ton. When the LCA and TEA results were integrated, we observed that the CO_2 physical activation pathway had a lower environmental impact (in terms of CO_2 eq.) and a higher economic benefit for industrial-scale applications (Fig. 4) compared with those of the two chemical activation pathways.

Discussion

Based on these observations and lab-scale experimental data (detailed discussion in ESI†), we conclude that upcycling waste PET plastic bottles into porous carbons offer a promising pathway. Given the mechanism and regeneration process underlying porous carbon-based CO_2 capture, adsorption–desorption can be widely achieved using PSA, TVSA, and other standard processes of temperature swing adsorption and
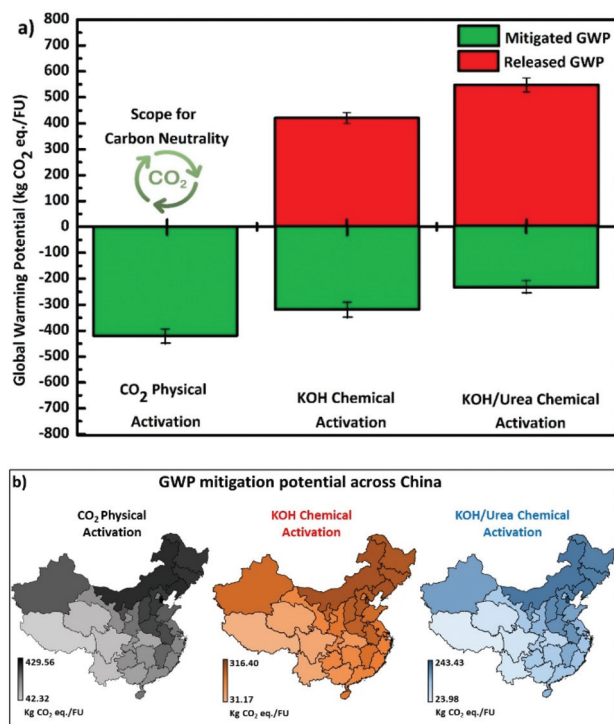
Fig. 5 Global warming potential (GWP) impacts. (a) Comparison showing the released and mitigated GWP for the three activation methods; (b) potential GWP reduction across China under the CO_2 physical, KOH chemical, and KOH/urea chemical activation methods. Planning such WPDPC production units favors China, especially for the provinces whose GWP for electricity production is higher.

vacuum pressure swing adsorption. Among these cyclic processes, TVSA has two major advantages:[69,70] (1) it requires mild operating conditions for sorbent regeneration, which can be driven by low-grade thermal solar energy, and (2) it has high CO_2 productivity. Therefore, based on CO_2 adsorption data, we designed a TVSA process to evaluate the steady-state cyclic performance and verified that all three WPDPCs are promising materials for CO_2 adsorption. We also confirmed that TVSA using PET6-KU7 exhibited the best CO_2 adsorption performance, as demonstrated by the industrial indicators and the highest energy conversion efficiency. However, PSA was considered for adsorbent regeneration when scaling up for industrial CO_2 capture processes, as it has been more widely commercialized than the other three typical processes.[71] Our assessment of the different adsorption processes can provide practical guidelines for developing industrial-scale CO_2 capture processes using WPDPCs.

We comprehensively performed both LCA and TEA based on industrial-scale process modeling data. Our findings confirm that for the KOH chemical and KOH/urea activation pathways, the variations in impact categories occur because of the presence of urea (26.16% of the CO_2 GWP) and its associated life-cycle impacts. The lowest environmental impacts were observed for the physical activation pathway because the CO_2 separated during PSA could be re-utilized as the activating

agent to produce PET6-CO_2-9. Our analysis also revealed that implementing such industrial plants based on the CO_2 physical activation method can be feasible to attain carbon neutrality. Additionally, in the CO_2 physical activation method, we observed the generation of by-products (water and char residue), which can be further used to promote industrial symbiosis-based eco-industrial parks, establishing that such plants could also promote carbon neutrality. In Fig. 5a, if we observe released emissions due to resource consumption in the activation process for the three WPDPCs, a clear difference is observed in the emissions released and mitigated based on the energy generation benefit offered by the PET waste valorization industry (see Fig. S8b† for details on other environmental impact categories). As a case study, we took one step ahead in estimating the GWP reductions across China considering the 23 provinces, 5 autonomous regions, and 4 municipalities; the observed CO_2 physical activation method has a strong potential for reducing the GWP from 42.32 to 429.56 kg CO_2 eq. per FU, compared with the two chemical activation methods (Fig. 5b). We believe that such plants could be beneficial for achieving carbon neutrality by 2060 in China.

The PSA process can also be used to separate CO_2 from the flue gas.[72] The use of CO_2 for activation is feasible for producing value-added products, such as WPDPCs. For example, CO_2 can be used as feedstock for higher hydrocarbons, thereby mitigating climate change,[73] aiding the conversion of flue gas to high-value carbons,[74] and reducing the usage of oil palm-derived activated carbon.[75] Moreover, the net economic benefits of industrial-scale WPDPC production using the three different pathways were verified. However, these economic benefits varied in the revenues generated, which depend on the selling price of porous carbons in the market and the heat-to-power conversion for electricity production (Fig. 6). As a case study, we based the prices of porous carbons on the Chinese market data (Table S10†). The production unit that used the CO_2 physical activation pathway to produce PET6-CO_2-9 was viable even when the porous carbon price fell below the minimum selling price by 30%–35% and an energy loss of approximately 75% occurred. The observed NPVs were positive for all 25 scenarios, ranging from €19.22 million to €48 million, and lay within the zone of feasibility (Fig. 4). The DPBP for PET6-CO_2-9 was significantly lower (~2 years), even in the worst-case scenario (a porous carbon selling price less than the minimum price and a loss of 75% of the heat that would otherwise be used to generate energy). The IRR was relatively high (68%–152%). The observed economic benefits of PET6-CO_2-9 physically activated by CO_2 gas make it more suitable for implementation in China. Such viable implementations could be considered as one of the promising net-zero carbon emission pathways. The production unit that used the KOH chemical activation pathway to produce PET6-K7 was viable only when the selling price of porous carbon did not fall below the market price. In addition, energy losses >50% resulted in a negative NPV. The observed NPV was between €−3.83 million and €26.65 million, with only 23 scenarios falling within the feasible zone (Fig. 4). The DPBP and IRR for
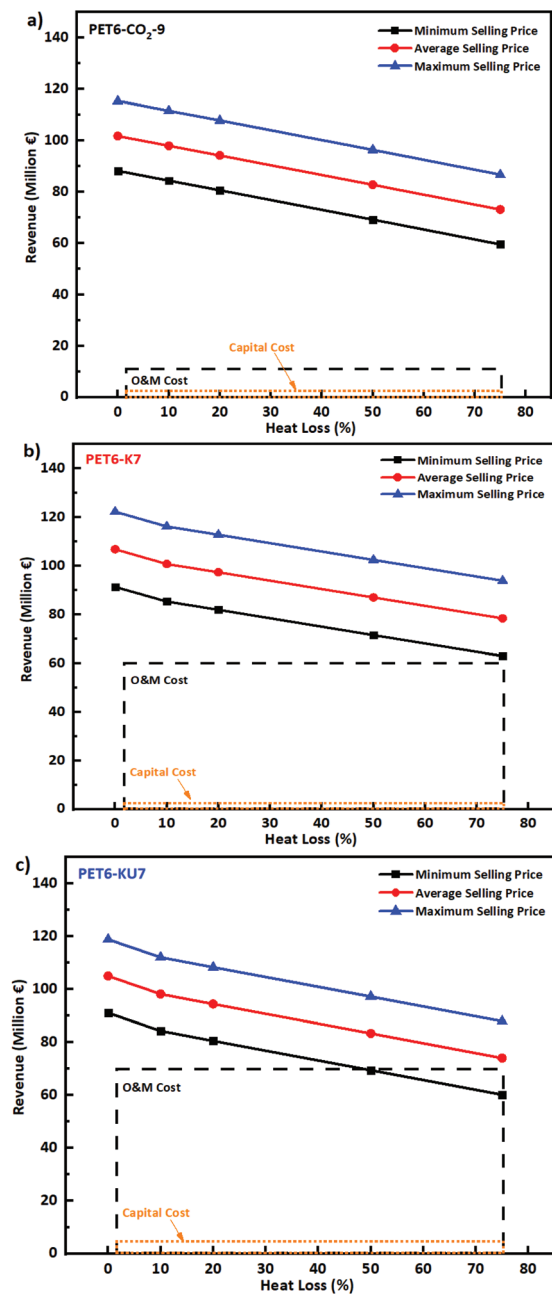
Fig. 6 Revenues from the industrial facility as a function of porous carbons selling price in the market and the heat loss for (a) PET6-CO₂-9, (b) PET6-K7, and (c) PET6-KU7. The generated revenues are cumulative of porous carbon sales and electricity sales under the sensitivity parameters (selling prices as shown in Tables S10 and S12†). For easy interpretation of the revenues earned and investment made in such plants, the operational and maintenance (O&M) (black dashed line) and capital (orange dotted line) costs are shown as rectangular boxes.

PET6-K7 varied from 1.25 to 12.1 years and from −11% to 90%, respectively. As the selling price fell below the minimum market price and the energy losses increased, the revenues decreased and significantly affected the NPV, which became negative (−383). The production unit that used the KOH/urea chemical activation pathway to produce PET6-KU7 was viable

only in 17 scenarios (Fig. 4). We observed that although the price of porous carbon could fall below the market value, the energy losses could not fall below 20%. The observed NPVs were between €−8.7 million and €21.56 million. The DPBP and IRR for PET6-KU7 varied from 1.51 years to more than its lifetime and from −13% to 75%, respectively. Overall, the TEA results suggest that all three pathways can produce porous carbons, even at low selling prices, given that the CHP plant maintains its excess electricity sales at a minimum of 50% by converting usable heat to power. Fig. S9† shows the selection of an activation pathway that is economically feasible and has a lower environmental impact. The integrated LCA and TEA findings indicate that the three proposed pathways offer viable alternatives to conventional CO_2 absorption technologies, owing to their characteristics of sustainable waste management, low environmental impact, and high economic feasibility.

Conclusions

The implementation of more effective and efficient actions to prevent threats from anthropogenic climate change and ubiquitous plastic pollution needs immediate attention. In this study, the upcycling of waste PET plastic bottles into value-added porous carbons for CO_2 capture was performed to mitigate these two major environmental issues simultaneously. The valorization of waste plastic into high-performance CO_2 adsorbents was verified as a sustainable and promising route for industrial-scale applications from the perspectives of both environmental impact and economic feasibility. The physical CO_2 activation approach was found to perform better than the two chemical activation pathways in terms of carbon emissions, providing a solution to achieving carbon neutrality and economic viability (NPV of €19.22 million over the project's operating life). Moreover, the trade-off strategies for the synthesis method and CO_2 capture performance were well-elaborated in different scenarios using LCA and TEA. Owing to the environmental benefits and economic feasibility of this approach, we highlighted it as a potential multifunctional alternative to conventional CO_2 absorption and plastic waste management technologies. With concerted effort on this novel application, it will be beneficial for achieving the SDGs of the UN.

Author contributions

X. Yuan – conceptualization, investigation, visualization, writing – original draft, review & editing; N. M. Kumar and B. Brigljević – data curation, software, visualization, writing – original draft, review & editing; S. Li, M. Byun, and B. Lee – software, data curation, formal analysis; S. Deng, C. S. K. Lin, D. C. W. Tsang, and K. B. Lee – supervision, writing – review & editing; S. S. Chopra and H. Lim – supervision, visualization, validation, writing – original draft, review & editing; Y. S. Ok –

supervision, visualization, validation, funding acquisition, writing – original draft, review & editing.

Conflicts of interest

There are no conflicts to declare.

Acknowledgements

Notes and references

1 X. Yuan, J. G. Lee, H. Yun, S. Deng, et al., Chem. Eng. J., 2020, 397, 125350.
2 J. Wang, X. Yuan, S. Deng, et al., Green Chem., 2020, 22(20), 6836–6845.
3 M. C. Rillig, M. Ryo, A. Lehmann, C. A. Aguilar-Trigueros, et al., Science, 2019, 366, 886–890.
4 L. Jia, S. Evans and S. V. Linden, Nat. Commun., 2019, 10, 4582.
5 R. Geyer, J. R. Jambeck and K. L. Law, Sci. Adv., 2017, 3(7), e1700782.
6 X. Yuan, X. Wang, B. Sarkar and Y. S. Ok, The COVID-19 pandemic necessitates a shift to a plastic circular economy, Nat. Rev. Earth Environ., 2021, 2, 659–660.
7 X.-D. Sun, X.-Z. Yuan, Y. Jia, et al., Nat. Nanotechnol., 2020, 15, 755–760.
8 K. D. Cox, G. A. Covernton, H. L. Davies, et al., Environ. Sci. Technol., 2019, 53, 7068–7074.
9 M. W. Callaghan, J. C. Minx and P. M. Forster, Nat. Clim. Change, 2020, 10, 118–123.
10 N. Mac Dowell, P. S. Fennell, N. Shah and G. C. Maitland, Nat. Clim. Change, 2017, 7, 243–249.
11 X. Yuan, M. Suvarna, S. Low, P. D. Dissanayake, K. B. Lee, J. Li, X. Wang and Y. S. Ok, Environ. Sci. Technol., 2021, 55(17), 11925–11936.
12 Y.-M. Wei, K.-N. Kang, L.-C. Liu, et al., Nat. Clim. Change, 2021, 11, 112–118.
13 M. Bui and N. Mac Dowell, Carbon Capture and Storage, RSC Energy and Environment Series, 2020, 1–7.
14 OECD Environment Policy Papers, 2018, DOI: 10.1787/c5f7c448-en.
15 B. Kaur, R. K. Gupta and H. Bhunia, Microporous Mesoporous Mater., 2019, 282, 146–158.
16 B. Kaur, J. Singh, R. K. Gupta and H. Bhunia, J. Environ. Manage., 2019, 242, 68–80.
17 J. Sun, Y. Sun, Y. Yang, X. Tong and W. Liu, Appl. Energy, 2019, 242, 919–930.
18 X. Yuan, S. Li, S. Jeon, et al., J. Hazard. Mater., 2020, 399, 123010.
19 V. Gargiulo, A. Gomis-Berenguer, P. Giudicianni, et al., Energy Fuels, 2018, 32, 10218–10227.
20 N. Querejeta, M. V. Gil, C. Pevida and T. A. Centeno, J. CO_2 Util., 2018, 26, 1–7.
21 J. J. Manyà, B. González, M. Azuara and G. Arner, Chem. Eng. J., 2020, 345, 631–639.
22 G. Singh, I. Y. Kim, K. S. Lakhi, et al., J. Mater. Chem. A, 2017, 5, 21196–21204.
23 Y. Xu, Z. Yang, G. Zhang and P. Zhao, J. Cleaner Prod., 2020, 264, 121645.
24 M.-J. Kim, S. W. Choi, H. Kim, S. Mun and K. B. Lee, Chem. Eng. J., 2020, 397, 125404.
25 X. Zhang, S. Zhang, H. Yang, Y. Feng, et al., Chem. Eng. J., 2014, 257, 20–27.
26 M. Al-Zareer, I. Dincer and M. A. Rosen, Int. J. Hydrogen Energy, 2020, 45, 11577–11592.
27 C. Shi, M. Elgarni and N. Mahinpey, Chem. Eng. Sci., 2021, 233, 116364.
28 A. Tripodi, M. Compagnoni, E. Bahadori and I. Rossetti, J. Ind. Eng. Chem., 2018, 66, 176–186.
29 J. Lorenzo-Llanes, J. Pagés-Díaz, E. Kalogirou and F. Contino, J. Environ. Chem. Eng., 2020, 8, 103540.
30 R. Tavares, E. Monteiro, F. Tabet and A. Rouboa, Renewable Energy, 2020, 146, 1309–1314.
31 C. Likkasit, A. Maroufmashat, A. Elkamel, H.-M. Ku and M. Fowler, Energy Convers. Manage., 2018, 168, 395–406.
32 E. Shagdar, B. G. Lougou, Y. Shuai, et al., RSC Adv., 2020, 10, 12582–12597.
33 N. Monnerie, P. G. Gan, M. Roeb and C. Sattler, Int. J. Hydrogen Energy, 2020, 45, 26117–26125.
34 B. Brigljević, M. Byun and H. Lim, Appl. Energy, 2020, 274, 115314.
35 S. Sgouridis, M. Carbajales-Dale, D. Csala, M. Chiesa and U. Bardi, Nat. Energy, 2019, 4, 456–465.
36 United Nation Sustainable Development Goals, 2015, https://sdgs.un.org/2030agenda.
37 B. Chen, S. Deng, L. Zhao, S. Li, et al., Sol. Energy, 2020, 209, 628–645.
38 L. Joss, M. Gazzani, M. Hefti, D. Marx and M. Mazzotti, Ind. Eng. Chem. Res., 2015, 54, 3027–3038.
39 L. Joss, M. Gazzani and M. Mazzotti, Chem. Eng. Sci., 2017, 158, 381–394.
40 Aspen Plus Technology, 2000, https://web.ist.utl.pt/ist11038/acad/Aspen/AspUserGuide10.pdf.
41 J. G. Hayden and J. P. O'Connell, Ind. Eng. Chem. Process Des. Dev., 1975, 14, 209–216.

42 C. A. Meyer, *et al.*, *ASME Steam Tables*, American Society of Mechanical Engineers, New York, 6th edn, 1993, ISBN: 0791806324.

43 A. Yang, Y. Su, W. Shen, I. L. Chien and J. Ren, *Energy Convers. Manage.*, 2019, **199**, 112041.

44 G. Soave, *Chem. Eng. Sci.*, 1972, **27**, 1197–1203.

45 A. Péneloux, E. Rauzy and R. Fréze, *Fluid Phase Equilib.*, 1982, **8**, 7–23.

46 E. Ansah, L. Wang and A. Shahbazi, *Waste Manage.*, 2016, **56**, 196–206.

47 S. Du, J. A. Valla, R. S. Parnas and G. M. Bollas, *ACS Sustain. Chem. Eng.*, 2016, **4**, 2852–2860.

48 J. Lee, T. Lee, Y. F. Tsang, J.-I. Oh and E. E. Kwon, *Energy Convers. Manage.*, 2017, **148**, 456–460.

49 J. Chattopadhyay, T. S. Pathak, R. Srivastava and A. C. Singh, *Energy*, 2016, **103**, 513–521.

50 M. Pohořelý, M. Vosecký, P. Hejdová, *et al.*, *Fuel*, 2006, **85**, 2458–2468.

51 D. Oh, H. W. Lee, Y.-M. Kim and Y.-K. Park, *Energy Procedia*, 2018, **144**, 111–117.

52 L. Chen, S. Wang, H. Meng, Z. Wu and J. Zhao, *Energy Procedia*, 2017, **105**, 391–397.

53 R. K. Singh, B. Ruj, A. K. Sadhukhan and P. Gupta, *J. Energy Inst.*, 2020, **93**, 1020–1035.

54 M. Azam, S. S. Jahromy, W. Raza, *et al.*, *Environ. Int.*, 2020, **134**, 105291.

55 A. Dhahak, V. Carre, F. Aubriet, G. Mauviel and V. Burkle-Vitzthum, *Ind. Eng. Chem. Res.*, 2020, **59**, 1495–1504.

56 A. Dhahak, G. Hild, M. Rouaud, G. Mauviel and V. Burkle-Vitzthum, *J. Anal. Appl. Pyrolysis*, 2019, **142**, 104664.

57 M. Dzięcioł and J. Trzeszczyński, *J. Appl. Polym. Sci.*, 2001, **81**, 3064–3068.

58 NETZSCH-Gerätebau GmbH, 2008, http://www.netzsch.com.

59 Ecoinvent database, 2021, https://www.ecoinvent.org/.

60 Agri-footprint database, 2021, https://www.agri-footprint.com.

61 S. You, W. Li, W. Zhang, H. Lim, *et al.*, *Crit. Rev. Environ. Sci. Technol.*, 2020, 1–29, DOI: 10.1080/10643389.2020.1848170.

62 T. Haeldermans, L. Campion, T. Kuppens, *et al.*, *Bioresour. Technol.*, 2020, **318**, 124083.

63 Y. Yang, J. Wang, K. Chong and A. V. Bridgwater, *Energy Convers. Manage.*, 2018, **174**, 406–416.

64 L. Shao, M. Liu, J. Huang and Y. N. Liu, *J. Colloid Interface Sci.*, 2018, **513**, 304–313.

65 D. Chen, Y. Fu, W. Yu, G. Yu and C. Pan, *Chem. Eng. J.*, 2018, **334**, 900–906.

66 H. A. Patel, J. Byun and C. T. Yavuz, *ChemSusChem*, 2017, **10**, 1303–1317.

67 B. Liu, S. Deng, S. Li, *et al.*, *Sep. Purif. Technol.*, 2019, **227**, 115670.

68 R. Zhao, L. Liu, L. Zhao, S. Deng, *et al.*, *Renew. Sust. Energy Rev.*, 2019, **114**, 109285.

69 L. Wang, Y. Yang, W. Shen, X. Kong, *et al.*, *Ind. Eng. Chem. Res.*, 2013, **52**, 7947–7955.

70 S. Li, S. Deng, R. Zhao, L. Zhao, *et al.*, *Energy*, 2019, **179**, 876–889.

71 A. D. Wiheeb, Z. Helwani, J. Kim and M. R. Othman, *Sep. Purif. Rev.*, 2015, **45**, 108–121.

72 B.-K. Na, H. Lee, K.-K. Koo and H. K. Song, *Ind. Eng. Chem. Res.*, 2002, **41**(22), 5498–5503.

73 C. Vogt, M. Monai, E. B. Sterk, *et al.*, *Nat. Commun.*, 2019, **10**, 5330.

74 W. Hago, *US patent*, 20210008496, 2020, Hago Energetics, Inc.

75 J. Y. Lai, L. H. Ngu, S. S. Hashim, J. J. Chew and J. Sunarso, *Carbon Lett.*, 2021, **31**, 201–252.